Pseudomonas syringae Type-III Secreted Effectors Elicit Unique Transcriptional Responses In *Arabidopsis thaliana*

Nicholas Garcia[1], Pauline Wang[1,2], Calvin Mok[1,2], Darrell Desveaux[1], and David Guttman[1,2]

[1]Department of Cell & Systems Biology, University of Toronto
[2]Centre For The Analysis Of Genome Evolution & Function

April 14, 2025

Abstract

Little is understood about the mechanisms of the majority of *Pseudomonas syringae*'s type III secreted effector repertoire, so here we developed a proof-of-principle methodology to characterize them based on the transcriptional response they individually elicit in the host.

Using the PtoDC3000D36E knockout strain to individually administer HopAB1 (AvrPtoB), HopB1, and HopN1 into *Arabidopsis thaliana*, we demonstrated that at 1 h and 8 h after infection each effector induces a unique transcriptional response that serves as a 'transcriptional fingerprint'. Furthermore, each transcriptional fingerprint was shown to significantly correlate with its corresponding effector's sub-cellular localization, functional mechanism, and targets.

We believe that these findings will allow for transcriptional fingerprints to guide future research into effector functionality *in planta*, and shed new light on those already partially characterized.

Acknowledgements

We thank the members of the Guttman and Desveaux laboratories for their invaluable guidance, feedback, and advice throughout this project, with particular thanks to Dr Crystal Su for her mentorship in fundamental microbiology protocols and plant care. We also thank Tamar Av-Shalom for her instruction in pressure infiltration technique. We would also like to thank Dr Yunchen Gong for his help in transfering sequence data for our analysis, and to Dr Tatiana Ruiz-Bedoya for saving us valuable time by having conjugated the DC3000 wildtype-representative PsyTEC alleles from *E. coli* into D36E previously.

Contents

List of Figures

List of Tables

0.1 Introduction

0.1.1 Background

Pseudomonas syringae is one of the most destructive and widespread plant pathogens that affect modern agriculture. Infecting a huge variety of plant species via its large family of strains, the gram-negative bacterium is responsible for billions of lost dollars in crop damage every year. From this variety of strains, *P. syringae* pv. *tomato* DC3000 has become the *de facto* model strain due to its unique ability to infect the model plant species *Arabidopsis thaliana*; creating a model *system* for studying plant-pathogen interaction.

A. thaliana utilises a bicameral immune response to defend against pathogens like DC3000. First, pathogen-associated molecular patterns (PAMP), for example flagellin proteins, are recognized by respective cell wall-bound pattern recognition receptor (PRR) proteins [Laflamme et al., 2020, Xin et al., 2018]. Upon recognition, PRRs trigger a gene expression pattern called PAMP-triggered immunity (PTI), a form of innate (basal) immunity [Laflamme et al., 2020, Bjornson et al., 2021]. PTI helps inhibit *P. syringae* growth by inducing reactive oxygen species (ROS) bursts via the respiratory burst oxidase homolog D (RBOHD) protein, alongside other defense mechanisms such as transcriptional reprogramming and callose deposition [Bjornson et al., 2021]. Following ROS bursting, botrytis-induced kinase 1 (BIK1) and brassinosteroid insensitive 1-associated receptor kinase 1 (BAK1), among other molecules, contribute to immune signaling cascades that lead to transcriptional up-regulation of various defense genes [Xin et al., 2018, Bjornson et al., 2021]. In the context of biotrophic or hemibiotrophic pathogens like *P. syringae* infection, the PTI response also prioritizes salicylic acid (SA) signalling over jasmonic acid (JA) signalling, as the former is more effective for defence against bio- and hemi-biotrophs like *P. syringae*, and vice-versa [Xin et al., 2018, Bjornson et al., 2021]. Evidence for this SA prioritization can be found in the up-regulation of pathogenesis-related 1 (PR1, a marker gene for SA signalling) and isochorismate synthase 1 (ICS1, a rate-limiting enzyme in SA biosynthesis) [Xin et al., 2018, Bjornson et al., 2021]. Ultimately, because SA and JA pathways are antagonistic due to resource allocation trade-offs, anti-*P. syringae* PTI also exhibits down-regulation of vegetative storage protein 2 (VSPT2) and lipoxygenase 2 (LOX2), key components of the JA pathway [Xin et al., 2018, Bjornson et al., 2021].

Given the perpetual arms race host-pathogen systems participate in, *P. syringae* evolved to evade pattern-triggered immunity using its type-III secretion system (T3SS). DC3000's T3SS injects a set of 36 type-III secreted effectors (T3SE) into plant cells to collaboratively suppress the PTI response and thus enable growth. The functions and targets of most of DC3000's individual effectors are largely unknown. If they become known, phytoimmune treatments could be developed for *A. thaliana* to prevent *P. syringae* growth, a solution that could eventually be designed to work in cash crops.

Eventually, *A. thaliana* evolved another layer of immunity against *P. syringae* called effector-triggered immunity (ETI). ETI is *A. thaliana*'s second line of defence against PTI-subverting pathogens like DC3000 and depends on nucleotide-binding leucine-rich repeat (NLR) proteins to detect effector activity [Laflamme et al., 2020]. Upon recognizing an effector, NLRs can trigger amplified immune outputs including hypersensitive response (HR)-associated cell death in some cases, though HR is not strictly required for pathogen growth restriction [Laflamme et al., 2020]. Transcriptional reprogramming during ETI exhibits intensified SA pathway dominance, with PR1 and ICS1 induction magnitudes exceeding PTI benchmarks by 3-5 fold [Yuan et al., 2021]. This binary de-

tection system, combining broad-spectrum PTI with NLR-mediated effector surveillance, creates overlapping immune gradients that DC3000's T3SE arsenal has evolved to suppress [Laflamme et al., 2020, Kvitko et al., 2009].

Model System

Currently, one of the most valuable research platforms available for studying individual effectors *in planta* is *P. syringae* pv. *tomato* DC3000D36E [Wei et al., 2015, 2018]. Developed by Wei and Collmer [2018], DC3000D36E (henceforth referred to as *D36E*) is a mutant of DC3000 with all of its T3SE genes silenced, effectively disarming the bacterium without affecting the T3SS itself [Wei et al., 2015, 2018]. Because its T3SS is still operational, D36E will still secrete any T3SE it is programmed to transcribe [Wei et al., 2015, 2018]. This fact allows D36E to serve as a test bed for D36E function by allowing for a controlled administration of individually transcribed effectors, should one be inserted into the bacterium via a genetic vector.

A comprehensive, standardized library of plasmid vectors carrying *P. syringae* effectors was developed by Laflamme et al. [2020]: the *P. syringae* Type III Effector Compendium (PsyTEC). It was developed by reducing a pan-genomic set of 5127 effector sequences from 494 *P. syringae* strains down to a set of 529 synthetic *representative alleles*, spanning the entire pan-genome effector diversity of *P. syringae* [Laflamme et al., 2020]. This library of representative alleles, stored on plasmid vectors in *Escherichia coli*, allow for reproducible, standardized assays with *P. syringae* effectors while minimizing strain-to-strain variation in effector composition. Ruiz-Bedoya et al. [2023] then successfully conjugated each PsyTEC plasmid representing DC3000 T3SE alleles into D36E hosts, and demonstrated that D36E's T3SS could secrete PsyTEC a single type of effector from a plasmid. While they primarily used the D36E-*A. thaliana* system for studying emergent cooperative virulence from effector repertoire (effectorome) composition, the system developed by Ruiz-Bedoya et al. [2023] served as a solid platform for designing single-effector assays to study DC3000 effector function.

0.1.2 Hypothesis

We hypothesized that each DC3000 effector, carried on a plasmid in D36E, individually triggers a unique set of response genes in *A. thaliana* upon infection, comprising an expression profile, depending on the effectors function. If true, this hypothesis carries significant implications:

1. Every DC3000 T3SE has a uniquely-identifiable "transcriptional fingerprint" that it elicits in *A. thaliana*.

2. A DC3000 T3SE's function could be predicted based on the transcriptomic patterns observed in its gene expression profile.

We tested this hypothesis using three D36E strains carrying PsyTEC DC3000 T3SE alleles that were conjugated by Ruiz-Bedoya et al. [2023]: D36E::HopN1a, D36E::HopB1a, and D36E::HopAB1j (HopAB1j is also known as AvrPtoB). These effector-carrying strains were chosen for three reasons: first, unlike most of the DC3000 effectorome, these three effectors have well-characterised behaviour and effects in *A. thaliana*. Second, if their transcriptional responses in *A. thaliana* align with their function, these three effectors

would allow us to further observe the *resolution* of their transcriptional responses. According to Xin et al. [2018], HopAB1 and HopB1 both localize at the plant cell membrane to target PRR signalling, whereas HopN1 localizes at the chloroplast to target programmed cell death. This difference in localisation between the two subsets of the three effectors would allow us to observe if the transcriptional responses elicited by each effector varied depending on where in the phytoimmune pathway they function. Furthermore, HopAB1 and HopB1 both target *different* PRRs: both target BAK1 but HopAB1 can also target FLS2 [Schreiber et al., 2021]. Because the two effectors differ in target *within the same locale*, differences in their gene expression profiles would demonstrate a 'transcriptional fingerprint' resolution great enough to differentiate individual effector targets. In short, D36E::HopN1a, D36E::HopB1a, and D36E::HopAB1j provide a convenient way to measure multiple levels of transcriptomic response resolution simultaneously based well-researched effector functions.

Predictions

We expected D36E, on its own, to elicit PTI as it, by design, lacks the effector repertoire necessary to evade it. Thus we expected a transcriptomic response from *A. thaliana* to follow the known gene expression patterns for PTI, being an up-regulation of genes related to defence and ROS production, and a down-regulation of genes in the jasmonic acid (JA) pathway. The specific gene markers we chose to look for were RBOHD (ROS burst), BIK1 (kinase signalling), BAK1 (PRR co-receptor), FRK1 (flagellin response), WRKY22/29 (transcription response), PR1 (SA marker) and ICS1 (SA biosynthesis) up-regulation, and LOX2 (JA biosynthesis), VSP2 (JA response), and JAZ1/10 (JA signalling repressors) down-regulation, as these markers capture the core PTI components (ROS burst function and SA and JA pathways) critical for anti-*P. syringae* immunity.

HopN1 principally degrades PsbQ, a critical component of photosystem II's oxygen-evolving complex, which suppresses ROS bursts during infection [Rodríguez-Herva et al., 2012]. ROS suppression in this manner likely contributes to observed down-regulation of ROS-responsive genes like RBOHD following D36E::HopN1a infection. Furthermore, by dampening ROS, HopN1 indirectly inhibits SA-dependent signalling. Thus, we expected to see down-regulation of ICS1 and PR1 following D36E::HopN1a infection, as these genes' expressions depend on SA signalling. Additionally, due to D36E::HopN1a's predicted SA pathway disruption, we expected to observe an up-regulation of LOX2 and VSP2. Finally, we also expected to observe an up-regulation in MC1 (metacaspase), as the chloroplast disruption induced by D36E::HopN1's PsbQ degradation triggers stress-induced programmed cell death through the antagonistically-enhanced JA pathway [Schreiber et al., 2021].

Because HopB1 targets membrane PRRs like BAK1 to suppress PTI signalling, we expected to observe a down-regulation of PTI markers compared to D36E::EV like RBOHD, FRK1, and WRKY22/29. Furthermore, because callose deposition is often impaired when PRR signalling is disrupted, we also expected to observe a down-regulation of CALS1 (a callose synthase), although its direct transcriptional regulation by BAK1 remains uncharacterized [Hong et al., 2001]. Additionally, PR1 and ICS1 down-regulation were expected due to HopB1's disruption of PRR-induced SA biosynthesis and signalling, alongside a complementary antagonistic up-regulation of LOX2 and VSP2 in the JA pathway.

HopAB1j acts as an E3 ligase targeting PRRs (like FLS2 and BAK1) for degradation, which disrupts PTI and SA signalling [Lu et al., 2011]. Consequently, we predicted

D36E::HopAB1j would elicit down-regulation of BAK1, FRK1, WRKY22/29, PR1, and ICS1 and up-regulation of LOX2 and VSP2, given HopAB1j's PRR-targeting E3 ubiquitin ligase behaviour. Additionally, we predicted an up-regulation of BAG6 (an anti-apoptotic chaperone protein). While the mechanistic link is speculative, we posited this because by degrading PRRs and E3 ligases (like PUB12/13), HopAB1j triggers endoplasmic reticulum (ER) stress, which activates cellular survival pathways like the unfolded protein response (UPR), which up-regulates BAG6, in an attempt to counter the effector-induced stress [Lu et al., 2011]. Finally, because HopAB1j-induced degradation of FLS2, we expected to observe a compensatory transcriptional down-regulation of FLS2 to avoid futile synthesis of what the plant perceives as a compromised receptor to occur, similarly to during miR172b/TOE1/2-mediated repression of FLS2 occurs [Zou et al., 2018].

It is worth noting that while we *expected* certain gene expression patterns, our expectations made up only a relatively miniscule portion of *A. thaliana*'s transcriptome, and there could have been far greater differences than anticipated.

Execution

Keeping these expected transcriptional responses in mind, we pressure-infiltrated each strain, suspended in 10 mM $MgSO_4$, into four-week-old *A. thaliana* plants in biological triplicate. As negative controls, we included identically prepared D36E::EV (empty vector, i.e., carrying no effector allele) and sterile $MgSO_4$ as a mock control. We then harvested and froze the infected leaves 1 h and 8 h post-infection, then extracted RNA from them and ran an RNA-seq pipeline for analysis.

0.2 Methods

0.2.1 Plant Preparation

Figure 1: 28 d old *A. thaliana* plants with their leaves marked to be infected with D36E::HopAB1 via pressure infiltration. Photo taken approximately 1 h before infection.

Figure 2: 28 d old *A. thaliana* plants with their leaves marked to be infected with D36E::HopB1 or $MgSO_4$ via pressure infiltration. Photo taken approximately 1 h before infection.

Figure 3: 28 d old *A. thaliana* plants with their leaves marked to be infected with D36E::HopN1 or D36E::EV via pressure infiltration. Photo taken approximately 1 h before infection.

Arabidopsis thaliana plants used in this study are in Col-0 ecotype background. The soil in which they were sown was prepared with fertilizer diluted in water at 1 ng/L. The plants were grown at 22 °C under a 12 h day-night cycle of 44 lamp intensity until they were 28 days old (sizes visible in figures 1, 2, and 3). They were watered every few days based on subjective judgement of soil surface dryness.

0.2.2 Bacteria Culturing

Two days before infection, D36E strains conjugated with the PsyTEC plasmid vectors of the three active treatments were streaked from a glycerol stock previously prepared by Ruiz-Bedoya et al.. D36E::EV was also streaked from a glycerol stock. Plating media was 50 % agar, 50 % King's B mix, with 50 µg/mL of rifampicin, and 100 µg/mL of kanamycin and streptomycin mixed in. The plates were then incubated at 30 °C overnight.

The day before infection, a sample of bacteria from each of the incubated plates were harvested with a pipette tip and suspended in a respective 400 µL volume of $MgSO_4$. The samples were mixed by moving the pipette tip up and down and swirling it until the solution became homogeneous, and then the volumes were pipetted onto respective new plates of identical media composition. The pipetted volumes were spread around the plates by placing 3-5 5 mm-diameter glass beads onto each plate and shaking vigorously. The plates were left to air dry in a biosafety cabinet until the solution no longer flowed when the plate was held sideways, and then incubated at 30 °C overnight.

0.2.3 Infection

Infiltrant preparation

To re-suspend the four overnight-incubated lawns of the treatment strains, 5 µL of $MgSO_4$ was added to each plate. The four plates were then shaken for 20 min at speed setting 500 on a plate shaker. Afterwards, the amalgamated lawns were gently scraped to suspend them in the $MgSO_4$ and then pipetted into respective microfuge tubes.

Each strain's 600 nm optical density was measured using a spectrophotometer by diluting 10 mL of it into 990 µL $MgSO_4$ in a cuvette. The recorded values were then multiplied by 100 to get the 600 nm optical density of the original undiluted sample.

Each sample was then diluted to a 600 nm optical density of 2.0. This was done by calculating the amount of $MgSO_4$ solvent that would be needed to dilute 400 µL of the strain to that optical density, using the following equation:

$$V_{MgSO_4} = C_{\text{undiluted sample}} \times V_{\text{strain}} - \frac{C_{\text{desired}} \times V_{\text{strain}}}{C_{\text{desired}}}$$

Where V_{strain} is the volume of the bacterial strain to dilute, V_{MgSO_4} is the volume of $MgSO_4$ to dilute V_{strain} into, $C_{\text{undiluted sample}}$ is the concentration of the undiluted sample (the 600 nm optical density of V_{strain}), and C_{desired} is the desired solution concentration following dilution (in this case, a 600 nm optical density of 2.0).

Once a 600 nm optical density of 2.0 was achieved for the four treatment solutions, they were serially $\frac{1}{10}$ diluted in $MgSO_4$ until four 50 mL volumes with 600 nm optical densities of 0.0002 remained, serving as the treatment infiltrants. 50 mL of leftover aliquoted $MgSO_4$ was additionally prepared in its own tube to be used as a mock treatment.

Infiltration

Pressure infiltration was conducted using disposable 10 mL syringes. For each treatment, three leaves per plant up to six plants were pressure infiltrated. The time of day was recorded upon infiltrating the last plant of a treatment. Infiltration for each treatment continued until 1 h had passed since completing the first round of infiltration. Upon reaching that timepoint, the leaves of three of that treatment's plants were cut at the petioles and stored into three tubes (one per plant). Each tube was immediately frozen in liquid nitrogen upon harvesting completion. This process of infiltration and leaf harvesting was repeated until all the 1 h post-infection leaves had been harvested and the remaining plants were still in-tact. 8 h after the recorded timepoint, the remaining plants were harvested in a similar manner.

The end result was 30 tubes, each containing 3 leaves of the same plant, where 15 tubes corresponded to the 1 h timepoint and the other 15 to the 8 h timepoint. Once harvesting was complete, all the tubes were stored at −80 °C.

0.2.4 RNA Extraction & Purification

All RNA extraction and purification methods were completed in an environment that was de-RNAsed 20 minutes in advance.

Tissue Homogenisation

Each of the thirty plant samples were ground into powder with a respective mortar and pestle that had been frozen via submersion in liquid nitrogen. The samples were then scraped into an open frozen microcentrifuge tube using a frozen metallic spatula, both of which had been similarly frozen via liquid nitrogen submersion. The tubes were then closed and frozen via liquid nitrogen submersion while the rest of the samples were similarly homogenized. In a fume hood, 1.5 mL of TRIzol was added to each tube, followed by an immediate vigorous manual shaking for 1 min. The tubes were then stored on ice.

Phase Separation

The TRIzol-suspended samples were centrifuged at 12 000 ×g for 10 min at 4 °C. The supernatants were then transferred into new respective 2 mL microcentrifuge tubes and incubated at room temperature (∼24 °C) for 5 min. In a fume hood, 300 µL of chloroform was added to each tube, followed by an immediate vigorous manual shaking of the tube for 15 s. The tubes were then incubated for 3 min at room temperature, and then centrifuged at 12 000 ×g for 15 min at 4 °C. The clear upper supernatant phase was then transferred into new respective microcentrifuge tubes.

Column Purification

Column purification was performed using the RNeasy™ Plant Mini Prep Kit. 1 volume of RLC buffer was added to each RNA aqueous solution and then inverted several times to mix. $\frac{1}{2}$ volumes of ethanol was added and once again inverted several times to mix. The solution was filtered through a pink RNeasy™ spin column at 7400 ×g for 15 s. After discarding the flow-through, 700 µL of RW1 buffer was then filtered through the column at 10 000 rpm for 15 s, with the flow-through being discarded. This was then repeated twice more with 2 × 500µL RPE buffer at 10 000 rpm, first for 15 s and then for 2 min. The columns were then transferred into new tubes and centrifuged at FULL SPEED for 1 min. Finally, the columns were transferred to new microcentrifuge tubes while ensuring they did not touch the flowthrough, and 90 µL of RNase-free water was spun through each of them to yield the purified RNA.

0.2.5 Sequencing

The purified RNA solutions were sequenced on an Illumina™ NextSeq 2000 by the Centre for the Analysis of Genome Evolution and Function (CAGEF).

0.2.6 Computation

Table 1: Utilized Bioinformatic Pipeline Software

Software Name	Version	Author(s)
R	4.4.2	R Core Team
FastQC	0.12.1	Andrews et al.
Trimmomatic	0.39	Bolger et al.
HISAT2	2.2.1	Kim et al.
SAMtools	1.21	Danecek et al.
featureCounts	2.0.8	Liao et al.
DESeq2	1.46.0	Love et al.
ggplot2	3.5.1	Wickham
org.At.tair.db	3.20.0	Carlson
AnnotationDbi	1.68.0	Pagès et al.
g:Profiler2	0.2.3	Kolberg et al.
pheatmap	1.0.12	Kolde
reshape2	1.4.4	Wickham
gridExtra	2.3	Auguie and Antonov
purrr	1.0.4	Wickham and Henry

Sequence Pre-Processing

A set of thirty `.fastq` files were outputted from the sequencer, comprising of three RNA sequences for each of the five treatments at each of the two timepoints. First, the quality of the sequences were verified by running them through FastQC version 0.12.1. Once all the sequence qualities were deemed good enough to continue, they were fed into Trimomatic version 0.39, with the `TRAILING` and `MINLEN` parameters set to `10` and `36`, respectively. The outputted trimmed files were then quality checked for the next step of the pipeline using FastQC.

Alignment and Counting

Using HISAT2 version 2.2.1, the pre-processed sequences were aligned to the 55$^{\text{th}}$ version of the *A.thaliana* TAIR10 reference genome developed by Yates et al.. This was done by first indexing the reference genome using HISAT2's `HISAT2-build` command to ensure efficient alignment, with the index files stored in a subdirectory called `indexes`. The name of each input `.fastq` file was then sanitized to remove spaces and special characters to ensure compatibility with downstream tools. Next, the paired-end sequencing reads were aligned to the indexed reference genome by executing the `HISAT2` command with the `-q` option enabled, the `-x` option pointing to the HISAT2 index in `indexes`, and the `-1` and `-2` options specifying the `R1` and `R2` paired-end read files, respectively. The output of HISAT2 was piped directly into `samtools sort` to generated sorted binary alignment map (BAM, `.bam`) files.

To count the mapped reads in the BAM files, they were ran through featureCounts version 2.0.8 with the `-p` (paired-end read counting) option enabled and the 55$^{\text{th}}$ version of the `A. thaliana` TAIR10 annotation (developed by Yates et al.) specified using the `-a` option. The raw count matrices were then processed using the UNIX `cut` command

to retain only columns 1 (containing the gene identifiers) and 7 (containing sample count data). This left three files as outputs: `output_data.txt`, `output_data.txt.summary`, and `clean_counts.txt`.

Differential Expression Analysis

The `clean_counts.txt` output file was used as the basis for the differential expression analysis powered by DESeq2 version 1.46.0. A metadata file was also manually written for this analysis step. The metadata file was a comma-separated values file with three columns labelled `sample_name`, `treatment`, and `timepoint`. The `sample_name` column contained the sample filenames listed in `clean_counts.txt` with the rest of the file name removed (e.g. `data/alignments/A10_S1.bam` was written as `A10_S1`). The `treatment` column contained the biological treatments associated with the samples in `sample_name` (e.g. "`HopB1a`", "`D36E_EV`", etc.). And the `timepoint` column contained the harvesting timepoints associated with the samples in `sample_name` (e.g. "`8h`" or "`1h`" for each sample).

In an R script, once `metadata.csv` was loaded using `read.table` with the header lines skipped and the row names set to gene identifiers to prepare a count matrix. The metadata was cleaned by renaming columns, updating treatment names to remove redundant suffixes (`e.g. HopN1a` $\rightarrow$ `HopN1`). Then, the metadata and count matrix were aligned to ensure consistent sample ordering, with samples not present in both datasets being removed.

Next, a DESeq2 object was created using the `DESeqDataSetFromMatrix` function, with the count matrix as `countData`, metadata as `colData`, and the following design formula: `treatment + timepoint + treatment:timepoint`. When it came time to actually execute the DESeq2 pipeline, it was executed sequentially. First, size factors were estimated to normalize library sizes. Then dispersion estimates were calculated, followed by an application of a negative binomial Wald test to fit the generalized linear model and test for differential expression. The final DESeq2 object was then saved for downstream analysis.

The first major differential expression analyses were the between-treatment timepoint comparisons. For each timepoint comparison, D36E::EV was compared to $MgSO_4$ at that timepoint. Each active treatment in that timepoint were then compared against D36E::EV and then had the DEGs from the aforementioned D36E::EV-$MgSO_4$ comparison filtered out. A data frame was then created for the results of the filtered comparison, with all of the DEGs with an adjusted p-value greater than 0.01 or a $\log_2$-fold change less than 2 removed. Finally, for ease of interpretation, TAIR locus identifiers were mapped to their corresponding gene symbols using R's `org.At.tair.db` (version 3.20.0) using the `mapIDs` function. It was employed with "TAIR" as the keytype and "SYMBOL" as the column option. If a single TAIR ID mapped to multiple gene symbols, the first listed symbol was selected (`multiVals = "first"`). Finally, a Manhattan plot and a volcano plot was generated and saved for each active treatment comparison.

The second major differential expression analyses were the within-treatment timepoint comparisons. These were conducted as simple pairwise comparisons between each active treatment's 8 h and 1 h timepoint data. For each treatment, a custom contrast was constructed combining the main time effect (`timepoint_8h_vs_1h`) with treatment-specific temporal interaction terms (e.g., `A10_S1.timepoint8h`), effectively modelling how each treatment's expression patterns evolve over time. Significant genes were filtered using the

same dual thresholds as in the between-treatment timepoint comparisons after filtering out non-applicable results. Volcano and Manhattan plots were also generated for each comparison as before.

Visualization

The `.csv` files generated by DESeq2 listing the filtered DEGs for each timepoint were imported for visualization using `read.csv`. For each of the two timepoints, DEG heatmaps were generated containing the three active treatments, followed by a gene ontology (GO) analysis, and concluded by the generation of a GO term heatmap.

To generate the DEG heatmaps, significant genes from each treatment comparison were combined into union lists per timepoint, with expression matrices being constructed with genes as rows and treatments as columns populated with $\log_2$-fold change values. The adjusted p-value threshold and absolute $\log_2$-fold change cutoff remained the same as before (0.01 and 2, respectively). To process the matrices while reducing noise, only genes with more than 2 observations across treatments were retained. Winsorization then capped extreme values at the 99^{th} percentile of the timepoint's $\log_2$-fold change distribution. Missing values were inputted as `0` to maintain matrix integrity. Next came the functional annotation, which involved functionally profiling gene clusters who had more than 5 members using `gProfiler2`. Enriched terms from GO Biological Processes, KEGG, and Reactome were identified with a $p < 0.05$ threshold and `g_SCS` correction method. The top terms per cluster were annotated directly onto the heatmap.

The last step before visualization was completed with the GO enrichment analysis. Genes were split into up-regulated/down-regulated sets for each treatment and adaptive minimum gene thresholds were applied (3 genes for HopN1, 5 for the other 1 h treatments, and 10 for the other 8 h treatments). A 3-attempt retry system with 5 s intervals was implemented for gProfiler queries, which included exclusion of root GO terms (biological process, molecular function, and cellular component). The result columns were then validated to ensure data integrity. This step concluded with the top 15 terms per data source being selected, their gene ratios being calculated ($\frac{\text{intersecting genes}}{\text{total query genes}}$), and appending the treatment/timepoint/direction data.

To generate the GO term heatmap from the GO enrichment analysis results, the first step was to aggregate $-\log_1 0(\text{p} - \text{values})$ across treatments into matrix format, followed by the creation of unique term identifiers combining ID and name. Next, terms with less than 1 valid observation, or a variance less than 0.1, were removed, following by a capping of extreme values at $\text{p} - \text{value} = 1 \times 10^{-20} \equiv -\log_1 0(\text{p} - \text{value}) = 20$. Finally, the original term order was preserved for biological interpretability, and the heatmaps were sized dynamically for readability ($\sim$0.3 mm per row).

After the GO term heatmaps were generated, the 1 h timepoint's heatmap was regenerated with the noise-reduction step retaining only genes with more than 1 observation across treatments, rather than 2 observations. This was because no heatmap could be generated for that timepoint otherwise, as so few DEGs were found.

0.3 Results

0.3.1 Sequencing

The 30 purified RNA samples had RNA integrity numbers (RIN) with values around 6.

0.3.2 Computational Metrics

Both before and after trimming, none of the sequences were flagged as poor quality by Trimmomatic. featureCounts alignment rates were all above 85 %.

0.3.3 DEGs by timepoint

Table 2: Genes significantly differentially expressed in *A. thaliana* in response to each active treatment comparison

Effector*	Time Post-Infection	Total	Induced	Repressed
HopN1a	1 h	2	1	1
HopN1a	8 h	14	4	10
HopB1a	1 h	1	1	0
HopB1a	8 h	960	659	301
HopAB1j	1 h	5	4	1
HopAB1j	8 h	543	474	69

* Administered aboard a D36E-conjugated plasmid vector and compared against D36E::EV.

Table 3: DEGs at 1 hour post-infection by effector treatment.

Effector*	Locus	Locale	Regulation	Product†
HopN1a	AT1G53035	Chloroplast	Up	Transmembrane protein
HopN1a	AT5G51720	Chloroplast	Down	NEET, involved in ROS homeostasis
HopB1a	AT2G45080	Cytoplasm	Up	Cyclin P3, enables protein kinase binding
HopAB1j	AT1G08630	Cytosol	Up	THA1, degrades Thr → Gly
HopAB1j	AT1G68050	Cytosol & nucleus	Up	FKF1, SCF ubiquitin ligase complex component
HopAB1j	AT1G06160	Nucleus	Up	ORA59, master regulator of JA pathway
HopAB1j	AT4G33980	Nucleus	Up	COR28
HopAB1j	AT3G48360	Nucleus	Down	BT2, part of TAC1-mediated telomerase pathway

* Administered aboard a D36E-conjugated plasmid vector and compared against D36E::EV.

† All information in this column was gathered from The Arabidopsis Information Resource (TAIR)

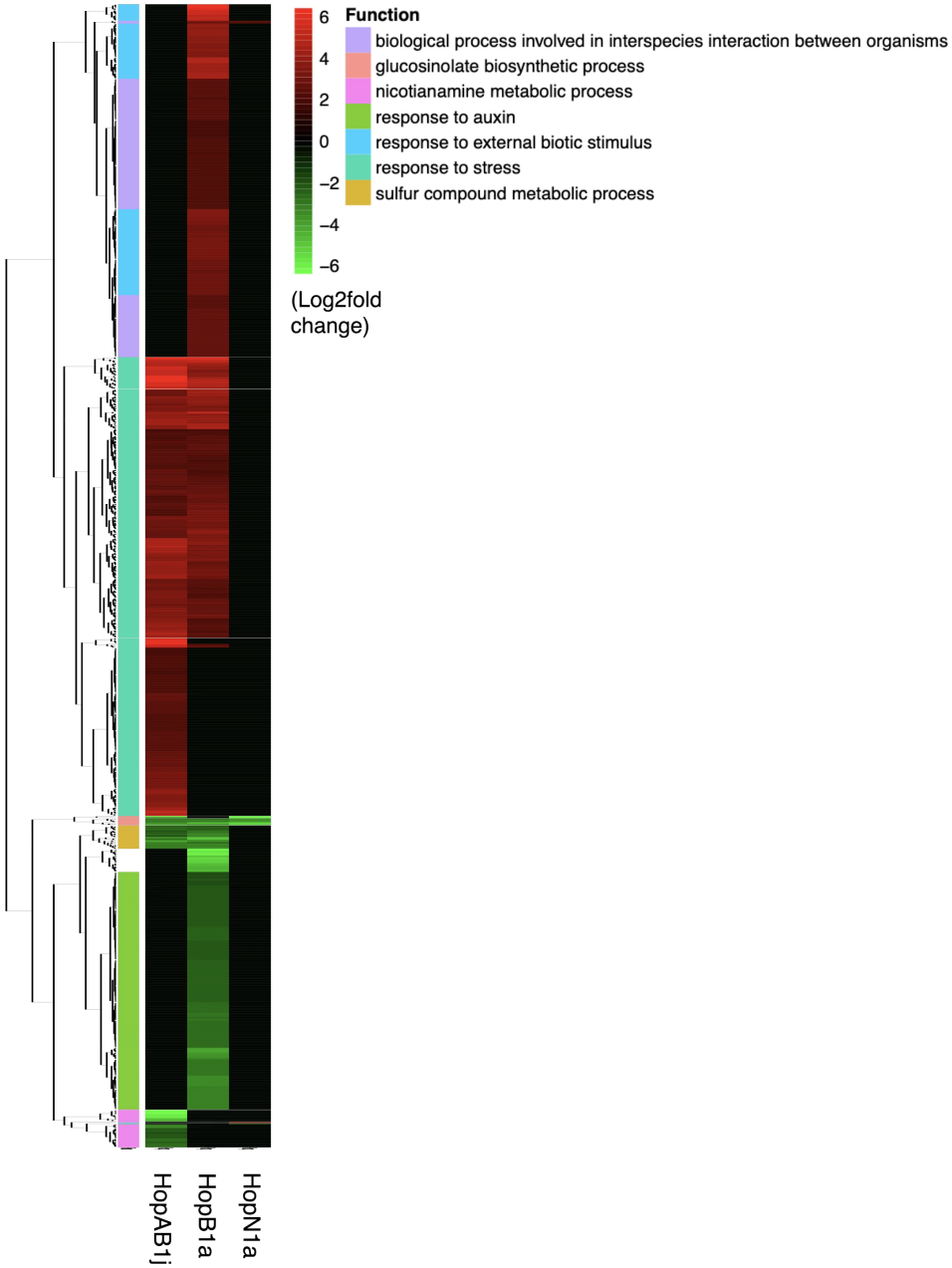

Figure 4: DEG patterns by treatment 8 hours post-infection. Effectors were administered aboard D36E-conjugated plasmid vectors. Only genes with more than 2 observations across treatments were included in this figure.

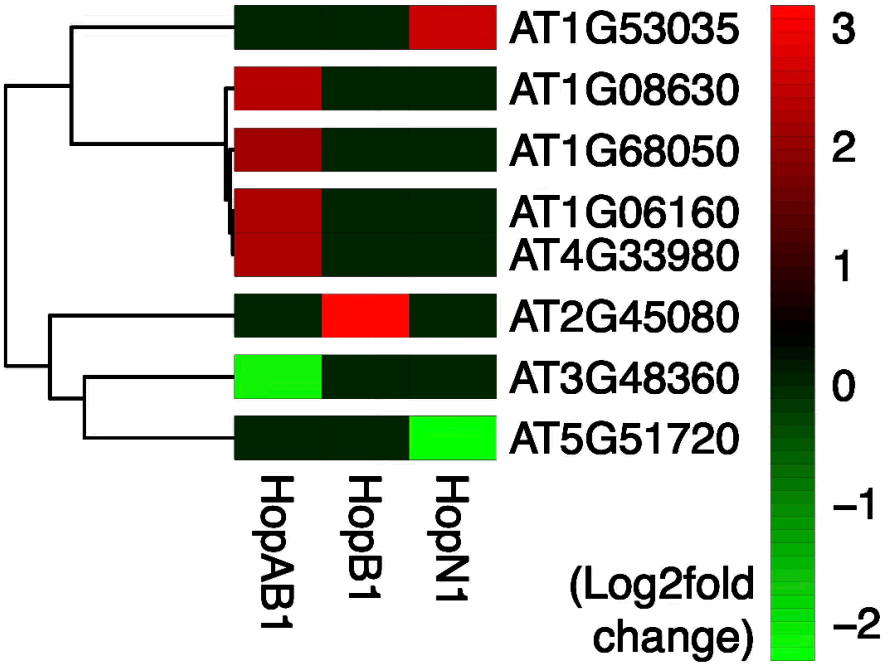

Figure 5: DEG patterns by treatment 1 hour post-infection. Effectors were administered aboard D36E-conjugated plasmid vectors.

Many hundreds of elicited DEGs were identified among the three active treatments at the 8 h timepoint, as can be seen in table 2. Describing the results of this timepoint with a resolution down to the individual DEG would be so grand as to be beyond the scope of this report. However, the high-level results of this timepoint, visible in figure 4, do possess notable results. D36E::HopB1a was observed to significantly down-regulate genes functionally characterised as relating to the plant's response to auxin, while significantly up-regulating genes characterised as relating to the plant's responses to stress and to external biotic stimuli, as well as relating to biological processes involved in interspecies interaction between organisms. The genes related to the plant's response to stress that were up-regulated by D36E::HopB1a were also observed to be but a subset of those similarly up-regulated by D36E::HopAB1j; demonstrating overlap in the induced responses of the two treatments. D36E::HopAB1j was also observed to significantly down-regulate genes related to the plant's sulfur compound metabolic process and its nicotianamine metabolic process. Finally, D36E::HopN1a induced only a relatively minuscule few dozen DEGs when compared to the other two treatments. These DEGs mostly related to the plant's biological processes involved in interspecies interaction between organisms.

When it came to the 1 h timepoint, a more manageable number of genes were found to be significantly differentially expressed. At this timepoint, D36E::HopB1a was found to only differentially express one gene locus: AT2G45080. This up-regulated gene encodes cyclin P3, cytoplasm-localized protein that enables protein kinase binding [Kaundal et al., 2010]. D36E::HopN1a on the other hand induced differential expression of two loci: it up-regulated AT1G53035 and down-regulated AT5G51720. AT1G53035 encodes a chloroplast-localized transmembrane protein and AT5G51720 encodes a chloroplast-localized NEET protein, which acts upstream or within the plant's ROS metabolic process [Kaundal et al., 2010, Nechushtai et al., 2012].

Finally, D36E::HopAB1j had the most diverse differential gene expression pattern of the three at this timepoint, up-regulating AT1G08630 (which encodes threonine aldolase 1, A.K.A. THA1), AT1G68050 (which encodes flavin-binding kelch repeat f box 1, A.K.A. FKF1), AT1G06160 (which encodes octadecanoid-responsive *Arabidopsis* AP2/ERF59, A.K.A. ORA59), and AT4G33980 (which encodes cold-regulated gene 28, A.K.A. COR28) while down-regulating AT3G48360 (which encodes BTB and TAZ domain protein 2, A.K.A. BT2) as well. THA1 enables, and acts upstream or within, the threonine catabolic process in the cytoplasm [Joshi et al., 2006], while FKF1 enables protein binding within the SCF ubiquitin ligase complex in the nucleus [Kim et al., 2007, Kuroda et al., 2012]. ORA59, perhaps the most significantly of all, enables DNA binding to regulate DNA-templated transcription in the nucleus [Fujimoto et al., 2000, Kaundal et al., 2010]; it is also a master regulator of the JA pathway, acting upstream or within the plant's response to jasmonic acid [Pré et al., 2008]. Furthermore, COR28 enables protein binding for a variety of processes, including negative regulation of DNA-templated transcription, in the nucleus [Li et al., 2020, 2016], while BT2, the sole protein down-regulated by D36E::HopAB1j at this timepoint, enables calmodulin and protein binding in the nucleus to contribute to DNA-binding transcription factor activity [Du and Poovaiah, 2004, Robert et al., 2009, Ren et al., 2007]. A summary of these DEGs induced by the three treatments can be found in table 3.

0.4 Discussion

0.4.1 Interpretation of Results

The Existence of 'Transcriptional Fingerprints'

Many hundreds (exact numbers available in table 2) of elicited DEGs were identified between the three active treatments at the 8 h timepoint. Due to time constraints, we were not able to perform an in-depth analysis of this timepoint's results down to the level of individual genes as such an endeavour's scope could comprise an entire future computational project of its own. However, the high-level results of this timepoint, visible in figure 4, do contain important patterns. Firstly, it is immediately apparent upon viewing figure 4 that unique patterns of differential gene expression were induced between the three effector treatments. This maintains a foundation of our hypothesis: that *A. thaliana*'s transcriptional response would differ between effector treatments. This point is further validated from the results of the 1 h timepoint shown in figure 5, where no two effector treatments had the same differential gene expression pattern (or, in more practical terms, none of the three columns are identical to eachother). These observations supports the idea that effector-induced transcriptional responses as a sort of "transcriptional fingerprint" that can serve as a unique identifying marker of a DC3000 effector in *A. thaliana*.

HopAB1

Due to the aforementioned time constraints, we primarily focused on the 1 h timepoint DEG data for the analysis of transcriptional fingerprint functional characterization. D36E::HopAB1 altered five DEGs at this timepoint, perhaps the most significant of which being its up-regulation of ORA59. HopAB1 is known to ubiquitinate JAZ proteins for proteasomal degradation, and by doing so liberates MYC2 transcription factors that are known to activate JA-responsive genes like ORA59. Thus, the observed up-regulation of ORA59 aligns with this behaviour, which suggests that HopAB1 is inducing JA to suppress the SA pathway via SA-JA antagonism. By suppressing SA, this pathway redirection would thus benefit the bacterium by repressing PTI. Moreover, this finding suggests that up-regulation of ORA59 can serve as a biomarker for HopAB1j's JAZ degradation activity, distinguishing it from HopB1 and HopN1. Furthermore, D36E::HopAB1j's up-regulation of FKF1, a part of the SCF ubiquitin ligase complex, could perhaps reflect an attempt by the host to compensate for HopAB1's E3 ubiquitin ligase activity. Therefore think an up-regulation of this gene in response to a pathogen effector may be a marker for the effector carrying out E3 ligase activity. Further *A. thaliana* post-infection transcription assays using other known E3 ubiquitin ligase activity-exhibiting effectors would be necessary to solidify this hypothesis.

Moving on to D36E::HopAB1j's up-regulation of COR28, this protein is known to repress circadian evening genes (PRR5, ELF4) that coordinate defence timing [Wang et al., 2017]. Therefore, up-regulation of this protein could repress the host's immune response by desynchronizing temperature-responsive immunity and the diurnal expression of pathogen-responsive genes. Another one of COR28's known functions is to promote hypocotyl elongation by repressing HY5's transcriptional activity through physical interaction with COP1 and HY5 [Li et al., 2020]. This suggests that part of HopAB1j's immune suppression strategy is to induce prioritization of host biomass production over host

defense—a common pathogen strategy to exploit metabolic resources. This suggested prioritization of growth over defense mirrors known BZR1-mediated trade-offs, where brassinosteroid signaling suppresses immunity to favor growth [Lozano-Durán et al., 2013].

Next, D36E::HopAB1j's up-regulation of THA1. THA1 catalyzes the reaction converting threonine into glycine and acetaldehyde [Joshi et al., 2006], the former serving as a precursor to glutathione (GSH)—a key antioxidant that neutralizes ROS produced during PTI [Zhu et al., 2021]. A larger host glycine pool could thus enhance GSH synthesis; thus by up-regulating THA1, HopAB1j is likely directly suppressing PTI by silencing the host's ROS bursts as part of its immune repression strategy. It is worth noting, however, that THA1's impact on glycine pools is likely tissue-specific and may be negligable in mature leaves. Furthermore, while GSH does scavenge ROS, its depletion in organelles is also known to be a defence signal. Thus, direct measurement of glycine and GSH levels in infected leaves at 1 h and 8 h may be necessary to clarify this potential aspect of HopAB1j's function.

Lastly in the scope of D36E::HopAB1j's induced DEGs at 1 h post-infection is its down-regulation of BT2. BT2 contains a BTB structural domain, which in other proteins facilitates the assembly of CUL3-based E3 ubiquitin ligases [Canning et al., 2013, Pintard et al., 2004]. If BT2 exhibits such facilitation, its downregulation by D36E::HopAB1j may be an attempt to alter host ubiquitination dynamics by interfering with the processes that target pathogen effectors for degradation. This could help HopAB1, with it's E3 ubiquitin ligase activity, evade host countermeasures by exploiting BT2, which would align with HopAB1's broader strategy of suppressing JA signalling and ubiquitin-mediated defences.

Regarding D36E::HopAB1j's induced DEGs at 8 h post-infection, its up-regulation of genes related to the host's response to stress can be attributed to a combination of mechanisms. HopAB1's E3 ubiquitin ligase activity, in disrupting proteostasis, could be activating the unfolded protein response (UPR) pathways, which up-regulates chaperone genes and endoplasmic reticulum stress genes. Similar host response behaviour has been observed in response to DSS1 mutants, which show heightened oxidative stress sensitivity; linking proteasome dysfunction to stress gene induction [Nikolic et al., 2023, 2021]. Furthermore, D36E::HopAB1j's previously-discussed PTI suppression via THA1 up-regulation to neutralize ROSs may have triggered ROS-responsive transcription factors in response to the disruption in redox homeostasis. Such redox-sensitive responses have been observed in *A. thaliana* during NADPH oxidase (RBOHD)-mediated immune signalling, where depletion of glutathione activates stress-related transcription factors independent of ROS accumulation [Schaubelt et al., 2014]. This also mirrors findings in *A. thaliana* DSS1 mutants, where proteasome dysfunction increases oxidative stress sensitivity despite antioxidant up-regulation [Lu et al., 2023]. In short, it seems as though the up-regulation in stress response genes at 8 h is a direct response to the effects of the DEGs induced at the 1 h timepoint. Furthermore, D36E::HopAB1j's down-regulation of genes related to nicotianamine metabolism at the 8 h timepoint could be due to a strategic homeostatic disruption of iron and zinc homeostasis. What we believe may be happening is that the THA1-up-regulation-driven glycine pool expansion, as discussed previously, may be leading to an increase in GSH. While GSH neutralizes ROS, it is also known to chelate metals [Haydon et al., 2012]. Thus, the down-regulation in nicotianamine synthesis could be the host compensating for this increased chelation to alter metal speciation. While DSS1-like proteasome dysfunction isn't addressed in the provided sources, the link between proteotoxic stress and glutathione-mediated metal chelation is supported by evidence that GSH depletion alters auxin signaling and root meristem development through

redox-regulated cell cycle control [Schaubelt et al., 2014].

HopB1

At the 1 h timepoint, D36E::HopB1a's up-regulation of cyclin P3 (CYCP3;1) was observed. CYCP3;1 is a P-type cyclin known to form complexes with CDKB2;1, which regulates the G2-M phase progression [Andriéu et al., 2008]. While there is no direct link between CYCP3;1 and RNA polymerase II phosphorylation, CDK12 is known to phosphorylate RNA polymerase II Ser2 residues to promote transcriptional elongation [Bartkowiak et al., 2010]. Thus, HopB1-induced up-regulation of CYCP3;1 could suggest two possible effects. One possibility is that an acceleration in RNA polymerase II phosphorylation could enable rapid transcription of stress-responsive genes like MYC2 or ERF1, amplifying JA and ethylene signaling pathways, which antagonize salicylic acid signaling similarly to HopAB1's up-regulation of ORA59, as discussed previously [Ngou et al., 2020]. Alternatively, CYCP3;1 up-regulation could indirectly lead to reduced Ser2 phosphorylation of RNA polymerase II, causing premature termination of immune-related transcripts such as PR1 and FRK1, thereby suppressing PTI [Rouvière et al., 2022]. We predict the latter is the more likely outcome, as it synergizes with HopB1's known protease activity and represents a more targeted mechanism, making it the more parsimonious hypothesis. To experimentally verify this hypothesis, phospho-Ser2 RNA Pol II ChIP-seq in D36E::HopB1a-infected versus control plants could identify premature termination at PR1/FRK1 loci. Additionally, RT-qPCR targeting 3' truncated transcripts could confirm incomplete elongation.

At the 8 h timepoint, D36E::HopB1a's significant down-regulation of genes related to the host's response to auxin aligns with its known protease activity targeting immune hubs. While HopB1 cleaves BAK1, a key immune co-receptor, there is no direct evidence that it targets auxin signaling components such as Aux/IAA proteins or ARF transcription factors. The observed auxin-related gene down-regulation may instead reflect indirect crosstalk between immune and auxin pathways. Furthermore, the shared up-regulation of genes related to the host's response to stress with D36E::HopAB1j (although notably fewer in D36E::HopB1a) aligns with the two effectors' distinct mechanisms: HopAB1 directly perturbs JA signaling [Li et al., 2016], while HopB1's cleavage of BAK1 triggers compensatory NLR-mediated defenses [Wu et al., 2020]. This simultaneous induction of stress genes and suppression of auxin-related pathways suggests that HopB1's broader strategy revolves around redirecting resources from growth to defense. Finally, the up-regulation of genes related to the host's response to external biotic stimuli and biological processes involved in interspecies interaction between organisms may reflect compensatory up-regulation of receptor-like kinases (RLKs). Because HopB1 is known to cleave BAK1, destabilizing immune receptor complexes, this could prompt feedback mechanisms involving RLKs, which are annotated as "interspecies interaction" in The Arabidopsis Information Resource (TAIR). To experimentally validate this hypothesis, we suggest future BAK1 cleavage assays and RLK phosphorylation profiling in D36E::HopB1a-infected *A. thaliana*.

HopN1

While little useful functional information was listed on TAIR regarding the AT1G53035 locus up-regulated by D36E::HopN1a at the 1 h timepoint, the other locus it induces differential expression in, AT5G51720 (NEET), is significant. Knowing that HopN1 works

to disrupt ROS burts by down-regulating targeting photosystem II with it's cysteine protease activity, the functional mapping of this DEG directly correlates with what we would have expected from its behaviour [Rodríguez-Herva et al., 2012].

Finally, D36E::HopN1's relatively few differentially expressed gene clusters at the 8 h timepoint can most likely be attributed to the effector targeting a more precise location in the host (the chloroplast) compared to the other two effectors. Ultimately, there is much more room to explore with the dataset of this timepoint. A crucial future direction, we suggest, is, for each treatment effector, to formulate possible functional hypotheses based on the observed DEG clusters, and verify them *in planta*. Alongside the suggested future directions we discussed previously for the 1 h timepoint findings, in-depth analysis beyond the scope of this proof-of-principle report can serve as a roadmap for further investigation. We furthermore suggest a future repetition of this experiment with a greater variety of timepoints, to see how variable the effector's observed transcriptional fingerprints may be between 0 h and 8 h. It would be of use to discover that the size of the transcriptional fingerprint (the number of DEGs) increases linearly over time, as it would allow for greater control over dataset size for analysis.

0.4.2 Limitations

RNA Extraction Quality

The most forefront limitation of this experiment was the RNA extraction. For unknown reasons (most likely related to manual technique) that months of troubleshooting was not able to resolve, the RNA samples extracted from the infected frozen leaf samples all yieled an RNA integrity number of around 6 (an ideal score would be 10, and the generally accepted minimum standard at CAGEF is around 7 for RNA sequencing). RNA integrity numbers generally decrease due to either contamination with genomic DNA or due to degradation. Our extracted RNA samples, upon closer inspection via an Agilent™TapeStation analyis, showed no genomic DNA contamination. And while it did show RNA degradation, the degradation was manageable enough so that we reasoned we would still be able to observe mRNA transcripts, as they tend to be shorter than the length of the observed degraded fragments.

Minimal Timepoints

This experiment was originally planned to observe the host transcriptional responses at more than two timepoints, but given the high cost of next-gen RNA sequencing, we had to compromise with just the 1 h and 8 h timepoints to stay within budget. This design choice was made while recognizing the potential response variances we were not able to observe.

0.5 Conclusion

This study provided compelling evidence that individual *Pseudomonas syringae* type-III secreted effectors elicit unique transcriptional responses in *Arabidopsis thaliana*, functioning as distinct "transcriptional fingerprints." By leveraging the DC3000D36E strain as a model platform for individual effector study, we demonstrated that the effectors HopN1, HopB1, and HopAB1 induce differential gene expression patterns reflective of their functional roles, cellular localization, and molecular targets in the host, affirming our hypothesis that each effector can be characterized via its transcriptional fingerprint, offering a novel approach for effector identification and functional prediction.

While this study focused on two timepoints (1 h and 8 h post-infection), future work could expand the temporal resolution to capture the full scope of gene expression change over time. Further experiments integrating proteomic and metabolomic analyses could complement the transcriptomic data generated in this study to provide a more comprehensive understanding of each effector's function. Ultimately, this comparative transcriptomic assay serves as a proof of principle for a novel framework for systematically characterizing type-III secreted effector function *in planta*.

Bibliography

Simon Andrews, Pierre Lindenbaum, Brian Howard, and Phil Ewels. Fastqc: a quality control tool for high throughput sequence data. Available online at http://www.bioinformatics.babraham.ac.uk/projects/fastqc/. Version 0.12.1, released March 01, 2023.

Jean-Pierre Andriéu, Del Carmen Martí, Ljung, Karin, Scofield, Steven, Fiers, Martijn, Beveridge, Christine, Leyser, Ottoline, and Nilsson, Ove. Requirement of b2-type cyclin-dependent kinases for meristem integrity and cell cycle progression in arabidopsis. *The Plant Cell*, 20(1):88–100, 2008. doi:10.1105/tpc.107.057612.

Baptiste Auguie and Anton Antonov. *gridExtra: Miscellaneous Functions for "Grid" Graphics*, 2017. URL https://CRAN.R-project.org/package=gridExtra. R package version: 2.3.

Bartlomiej Bartkowiak, Peng Liu, and Greenleaf, Arno L. The rna polymerase ii ctd coordinates transcription and rna processing through phosphorylation-dependent recruitment. *Genes & Development*, 26(19):2119–2133, 2010. doi:10.1101/gad.197545.110.

Marta Bjornson, Priya Pimprikar, Thorsten Nürnberger, and Cyril Zipfel. The transcriptional landscape of *Arabidopsis thaliana* pattern-triggered immunity. *Nature Plants*, 7: 579–586, 2021. doi:10.1038/s41477-021-00874-5.

Anthony M. Bolger, Marc Lohse, and Björn Usadel. Trimmomatic: a flexible trimmer for illumina sequence data. *Bioinformatics*, 30(15):2114–2120, 2014. doi:10.1093/bioinformatics/btu170. URL http://www.usadellab.org/cms/index.php?page=trimmomatic.

Peter Canning, Christopher D.O. Cooper, Tobias Krojer, James W. Murray, Ashley C.W. Pike, Apirat Chaikuad, Tracy Keates, Chancievan Thangaratnarajah, Viktorija Hojzan, Brian D. Marsden, Opher Gileadi, Stefan Knapp, Frank von Delft, and Alex N. Bullock. Structural basis for cul3 protein assembly with the btb-kelch family of e3 ubiquitin ligases. *Journal of Biological Chemistry*, 288(11):7803–7814, 2013. ISSN 0021-9258. doi:10.1074/jbc.m112.437996.

Marc Carlson. *org.At.tair.db: Genome wide annotation for Arabidopsis*, 2024. R package version: 3.20.0.

Petr Danecek, James K Bonfield, Jennifer Liddle, John Marshall, Valeriu Ohan, Martin O Pollard, Andrew Whitwham, Thomas Keane, Shane A McCarthy, Robert M Davies, and Heng Li. Twelve years of SAMtools and BCFtools. *GigaScience*, 10(2), 02 2021. ISSN 2047-217X. doi:10.1093/gigascience/giab008. giab008.

Linna Du and B. W. Poovaiah. A novel family of Ca^{2+}/Calmodulin-binding proteins involved in transcriptional regulation: Interaction with fsh/ring3 class transcription activators. *Plant Molecular Biology*, 54(4):549–569, 2004. doi:10.1023/B:PLAN.0000038269.98972.bb.

Susan Y. Fujimoto, Masaru Ohta, Akemi Usui, Hideaki Shinshi, and Masaru Ohme-Takagi. Arabidopsis ethylene-responsive element binding factors act as transcriptional activators or repressors of gcc box-mediated gene expression. *The Plant Cell*, 12(3): 393–404, March 2000. doi:10.2307/3870944.

Michael J. Haydon, Miki Kawachi, Markus Wirtz, Stefan Hillmer, Rüdiger Hell, and Ute Krämer. Vacuolar nicotianamine has critical and distinct roles under iron deficiency and for zinc sequestration in arabidopsis. *The Plant Cell*, 24(2):724–737, 2012. ISSN 1532-298X. doi:10.1105/tpc.111.095042.

Zonglie Hong, Ashton Delauney, and Desh Pal Verma. A cell plate–specific callose synthase and its interaction with phragmoplastin. *The Plant Cell*, 13:755–768, 2001. doi:10.1105/tpc.13.4.755.

Vijay Joshi, Karen M. Laubengayer, Nicolas Schauer, Alisdair R. Fernie, and Georg Jander. Two arabidopsis threonine aldolases are nonredundant and compete with threonine deaminase for a common substrate pool. *The Plant Cell*, 18(12):3564–3575, 2006. doi:10.1105/tpc.106.044958.

Rakesh Kaundal, Reena Saini, and Patrick X. Zhao. Combining machine learning and homology-based approaches to accurately predict subcellular localization in arabidopsis. *Plant Physiology*, 154(1):36–54, 2010. doi:10.1104/pp.110.156851.

Daehwan Kim, Joseph M. Paggi, Chanhee Park, Corey Bennett, Steven L. Salzberg, and Mihaela Pertea. Graph-based genome alignment and genotyping with hisat2 and hisat-genotype. *Nature Biotechnology*, 37(8):907–915, 2019. doi:10.1038/s41587-019-0201-4. Version: 2.2.1.

W.-Y. Kim, S. Fujiwara, S.-S. Suh, J. Kim, Y. Kim, L. Han, K. David, J. Putterill, H.-G. Nam, and D. E. Somers. Zeitlupe is a circadian photoreceptor stabilized by gigantea in blue light. *Nature*, 449:356–360, 2007. doi:10.1038/nature06132.

Liis Kolberg, Uku Raudvere, Ivan Kuzmin, Jaak Vilo, and Hedi Peterson. gprofiler2– an r package for gene list functional enrichment analysis and namespace conversion toolset g:profiler. *F1000Research*, 9 (ELIXIR)(709), 2020. R package version: 0.2.3.

Raivo Kolde. *pheatmap: Pretty Heatmaps*, 2018. URL `https://github.com/raivokolde/pheatmap`. R package version: 1.0.12.

Hirofumi Kuroda, Yuki Yanagawa, Naoki Takahashi, Yoko Horii, and Minami Matsui. A comprehensive analysis of interaction and localization of arabidopsis skp1-like (ask) and f-box (fbx) proteins. *PLOS ONE*, 7(11):e50009, 2012. doi:10.1371/journal.pone.0050009.

Brian Kvitko, Duck Hwan Park, André Velásquez, Chia-Fong Wei, Alistair Russell, Gregory Martin, David Schneider, and Alan Collmer. Deletions in the repertoire

of *Pseudomonas syringae* pv. *tomato* DC3000 type III secretion effector genes reveal functional overlap among effectors. *PLoS Pathogens*, 5(4):e1000388, 2009. doi:10.1371/journal.ppat.1000388.

Bradley Laflamme, Marcus Dillon, Alexandre Martel, Renan Almeida, Pauline Wang, Darrell Desveaux, and David Guttman. The pan-genome effector-triggered immunity landscape of a host-pathogen interaction. *Science*, 367(6479):763–768, 2020. doi:10.1126/science.aax4079.

Lei Li, Panya Kim, Liping Yu, Gaihong Cai, She Chen, James Alfano, and Jian-Min Zhou. Activation-dependent destruction of a co-receptor by a *Pseudomonas syringae* effector dampens plant immunity. *Cell Host & Microbe*, 20(4):504–514, 2016.

Xu Li, Cuicui Liu, Zhiwei Zhao, Dingbang Ma, Jinyu Zhang, Yu Yang, Yawen Liu, and Hongtao Liu. Cor27 and cor28 are novel regulators of the cop1–hy5 regulatory hub and photomorphogenesis in arabidopsis. *The Plant Cell*, 32(10):3139–3154, 2020. doi:10.1105/tpc.20.00195.

Yang Liao, Gordon Smyth, and Wei Shi. featurecounts: an efficient general-purpose read summarization program. *Bioinformatics*, 30(7):923–930, 2014. doi:10.1093/bioinformatics/btt656. URL `https://bioconductor.org/packages/release/bioc/html/Rsubread.html`. Version: 2.0.8.

Michael Love, Wolfgang Huber, and Simon Anders. Moderated estimation of fold change and dispersion for rna-seq data with deseq2. *Genome Biology*, 15(12):550, 2014. doi:10.1186/s13059-014-0550-8. R package version: 1.46.0.

Rosa Lozano-Durán, Alberto P Macho, Freddy Boutrot, Cécile Segonzac, Imre E Somssich, and Cyril Zipfel. The transcriptional regulator BZR1 mediates trade-off between plant innate immunity and growth. *eLife*, 2:e00983, 2013. doi:10.7554/eLife.00983.

Dongping Lu, Wenwei Lin, Xiquan Gao, Shujing Wu, Cheng Cheng, Julian Avila, Antje Heese, Timothy Devarenne, Ping He, and Libo Shan. Direct ubiquitination of pattern recognition receptor fls2 attenuates plant innate immunity. *Science*, 332(6036):1439–1442, 2011. doi:10.1126/science.1204903.

Ping Lu, Ke Wang, Jiaqi Wang, Chunbo Xia, Shu Yang, Liang Ma, and Haojie Shi. A novel zinc finger transcription factor, bcmsn2, is involved in growth, development, and virulence in botrytis cinerea. *Frontiers in Microbiology*, 14, October 2023. ISSN 1664-302X. doi:10.3389/fmicb.2023.1247072. URL `http://dx.doi.org/10.3389/fmicb.2023.1247072`.

Rachel Nechushtai, Andrea R. Conlan, Yael Harir, Luhua Song, Ohad Yogev, Yael Eisenberg-Domovich, Oded Livnah, Dorit Michaeli, Rachel Rosen, Vincent Ma, Yuting Luo, John A. Zuris, Mark L. Paddock, Zvi Ioav Cabantchik, Patricia A. Jennings, and Ron Mittler. Characterization of arabidopsis neet reveals an ancient role for neet proteins in iron metabolism. *The Plant Cell*, 24(5):2139–2154, May 2012. doi:10.1105/tpc.112.097634.

Bruno Pok Man Ngou, Ding, Pengbo, and Jones, Jonathan D.G. Mutual potentiation of plant immunity by cell-surface and intracellular receptors. *bioRxiv*, 2020. doi:10.1101/2020.04.10.034173. Preprint.

Ivana Nikolic, Jelena Samardzic, Strahinja Stevanovic, Jovanka Miljus-Dukic, Mira Milisavljevic, and Gordana Timotijevic. Crispr/cas9-targeted disruption of two highly homologous arabidopsis thaliana dss1 genes with roles in development and the oxidative stress response. *International Journal of Molecular Sciences*, 24(3):2442, 2023. ISSN 1422-0067. doi:10.3390/ijms24032442.

Ivana P. Nikolic, Sofija B. Nesic, Jelena T. Samardzic, and Gordana S. Timotijevic. Intrinsically disordered protein atdss1(v) participates in plant defense response to oxidative stress. *Protoplasma*, 258(4):779–792, 2021. ISSN 1615-6102. doi:10.1007/s00709-020-01598-7.

Hervé Pagès, Marc Carlson, Seth Falcon, and Nianhua Li. *AnnotationDbi: Manipulation of SQLite-based annotations in Bioconductor*, 2024. URL `https://bioconductor.org/packages/AnnotationDbi`. R package version: 1.64.1.

Lionel Pintard, Andrew Willems, and Matthias Peter. Cullin-based ubiquitin ligases: Cul3–btb complexes join the family. *The EMBO Journal*, 23(8):1681–1687, 2004. ISSN 1460-2075. doi:10.1038/sj.emboj.7600186. URL `http://dx.doi.org/10.1038/sj.emboj.7600186`.

Matthieu Pré, Mohamed Atallah, Anne Champion, Martin De Vos, Corné M. J. Pieterse, and Johan Memelink. The ap2/erf domain transcription factor ora59 integrates jasmonic acid and ethylene signals in plant defense. *Plant Physiology*, 147(3):1347–1357, 2008. doi:10.1104/pp.108.117523.

R Core Team. *R: A Language and Environment for Statistical Computing*. R Foundation for Statistical Computing, Vienna, Austria, 2024.

Shuxin Ren, Amanda J. Kerstetter, and Thomas D. McKnight. Regulation of telomerase in arabidopsis by bt2, an apparent target of TELOMERASE ACTIVATOR1. *The Plant Cell*, 19(1):23–31, 2007. doi:10.1105/tpc.106.044321.

Hélène S. Robert, Ab Quint, Daan Brand, Adam Vivian-Smith, and Remko Offringa. Btb and taz domain scaffold proteins perform a crucial function in arabidopsis development. *The Plant Journal*, 58(1):109–118, 2009. doi:10.1111/j.1365-313X.2008.03764.x.

José Rodríguez-Herva, Pablo González-Melendi, Raquel Cuartas-Lanza, María Antunez-Lamas, Isabel Río-Alvarez, Ziduo Li, Gema López-Torrejón, Isabel Díaz, Juan del Pozo, Suma Chakravarthy, Alan Collmer, Pablo Rodríguez-Palenzuela, and Emilia López-Solanilla. A bacterial cysteine protease effector protein interferes with photosynthesis to suppress plant innate immune responses. *Cellular Microbiology*, 14(5):669–681, 2012. doi:10.1111/j.1462-5822.2012.01749.x.

Jérôme O. Rouvière, Lykke-Andersen, Søren, and Jensen, Torben Heick. Control of non-productive rna polymerase ii transcription via its early termination in metazoans. *Biochemical Society Transactions*, 50(1):283–292, 2022. doi:10.1042/BST20210420.

Tatiana Ruiz-Bedoya, Pauline Wang, Darrell Desveaux, and David Guttman. Cooperative virulence via the collective action of secreted pathogen effectors. *Nature Microbiology*, 8:640–650, 2023. doi:10.1038/s41564-023-01328-8.

Daniel Schaubelt, Guillaume Queval, Yingping Dong, Pedro Diaz-Vivancos, Matome Eugene Makgopa, Gareth Howell, Ambra De Simone, Juan Bai, Matthew A. Hannah, and Christine H. Foyer. Low glutathione regulates gene expression and the redox potentials of the nucleus and cytosol in *Arabidopsis thaliana*. *Plant, Cell & Environment*, 38(2): 266–279, 2014. ISSN 1365-3040. doi:10.1111/pce.12252.

Karl Schreiber, Ilea Chau-Ly, and Jennifer Lewis. What the wild things do: Mechanisms of plant host manipulation by bacterial type iii-secreted effector proteins. *Microorganisms*, 9(5):1029, 2021. doi:10.3390/microorganisms9051029.

Peng Wang, Xuan Cui, Chunsheng Zhao, Liyan Shi, Guowei Zhang, Fenglong Sun, Xiaofeng Cao, Li Yuan, Qiguang Xie, and Xiaodong Xu. COR27 and COR28 encode nighttime repressors integrating *Arabidopsis* circadian clock and cold response. *J. Integr. Plant Biol.*, 59(2):78–85, 2017. doi:10.1111/jipb.12512.

Hai-Lei Wei and Alan Collmer. Defining essential processes in plant pathogenesis with *Pseudomonas syringae* pv *tomato* DC3000 disarmed polymutants and a subset of key type III effectors. *Molecular Plant Pathology*, 19(7):1779–1794, 2018.

Hai-Lei Wei, Suma Chakravarthy, Johannes Mathieu, Tyler Helmann, Paul Stodghill, Bryan Swingle, Gregory Martin, and Alan Collmer. *Pseudomonas syringae* pv. *tomato* DC3000 type III secretion effector polymutants reveal an interplay between hopAD1 and avrptoB. *Cell Host & Microbe*, 17(6):752–762, 2015. doi:10.1016/j.chom.2015.05.007.

Hai-Lei Wei, Wei Zhang, and Alan Collmer. Modular study of the type III effector repertoire in *Pseudomonas syringae* pv. *tomato* DC3000 reveals a matrix of effector interplay in pathogenesis. *Cell Reports*, 23(6):1630–1638, 2018. doi:10.1016/j.celrep.2018.04.037.

Hadley Wickham. Reshaping data with the reshape package. *Journal of Statistical Software*, 21(12):1–20, 2007. doi:10.18637/jss.v021.i12. URL `http://www.jstatsoft.org/v21/i12/`. R package version: 1.4.4.

Hadley Wickham. *ggplot2: Elegant Graphics for Data Analysis*. Springer-Verlag New York, 2016. ISBN 978-3-319-24277-4. URL `https://ggplot2.tidyverse.org`. R package version: 3.5.1.

Hadley Wickham and Lionel Henry. *purrr: Functional Programming Tools*, 2025. URL `https://CRAN.R-project.org/package=purrr`. R package version: 1.0.4.

Zhaoyang Wu, Min Li, Lijing Dong, Bin Xia, Dong Liu, and Jian-Min Zhou. Loss of the common immune coreceptor bak1 leads to nlr-dependent cell death. *Proceedings of the National Academy of Sciences*, 117(43):27044–27053, 2020. doi:10.1073/pnas.1915339117.

Xiu-Fang Xin, Brian Kvitko, and Sheng Yang He. *Pseudomonas syringae*: what it takes to be a pathogen. *Nature Reviews Microbiology*, 16(5):316–328, 2018. doi:10.1038/nrmicro.2018.17.

Andrew D. Yates, James Allen, Ridwan M. Amode, Andrey G. Azov, Matthieu Barba, Andrés Becerra, Jyothish Bhai, Lahcen I. Campbell, Manuel Carbajo Martinez, Marc Chakiachvili, Kapeel Chougule, Mikkel Christensen, Bruno Contreras-Moreira, Alayne Cuzick, Luca Da Rin Fioretto, Paul Davis, Nishadi H. De Silva, Stavros Diamantakis, Sarah Dyer, Justin Elser, Carla V. Filippi, Astrid Gall, Dionysios Grigoriadis, Cristina Guijarro-Clarke, Parul Gupta, Kim E. Hammond-Kosack, Kevin L. Howe, Pankaj Jaiswal, Vinay Kaikala, Vivek Kumar, Sunita Kumari, Nick Langridge, Tuan Le, Manuel Luypaert, Gareth L. Maslen, Thomas Maurel, Benjamin Moore, Matthieu Muffato, Aleena Mushtaq, Guy Naamati, Sushma Naithani, Andrew Olson, Anne Parker, Michael Paulini, Helder Pedro, Emily Perry, Justin Preece, Mark Quinton-Tulloch, Faye Rodgers, Marc Rosello, Magali Ruffier, James Seager, Vasily Sitnik, Michal Szpak, John Tate, Marcela K. Tello-Ruiz, Stephen J. Trevanion, Martin Urban, Doreen Ware, Sharon Wei, Gary Williams, Andrea Winterbottom, Magdalena Zarowiecki, Robert D. Finn, and Paul Flicek. Ensembl genomes 2022: an expanding genome resource for non-vertebrates. *Nucleic Acids Research*, 2022. doi:10.1093/nar/gkab1007.

Minhang Yuan, Zeyu Jiang, Guozhi Bi, Kinya Nomura, Menghui Liu, Yiping Wang, Boying Cai, Jian-Min Zhou, Sheng Yang He, and Xiu-Fang Xin. Pattern-recognition receptors are required for nlr-mediated plant immunity. *Nature*, 592(7852):105–109, 2021. doi:10.1038/s41586-021-03316-6.

Feng Zhu, Qi-Ping Zhang, Yan-Ping Che, Peng-Xiang Zhu, Qin-Qin Zhang, and Zhao-Lin Ji. Glutathione contributes to resistance responses to tmv through a differential modulation of salicylic acid and reactive oxygen species. *Molecular Plant Pathology*, 22(12):1668–1687, 2021. doi:10.1111/mpp.13138.

Yanmin Zou, Shuangfeng Wang, Yuanyuan Zhou, Jiaojiao Bai, Guozhong Huang, Xiaotong Liu, Yingying Zhang, Dingzhong Tang, and Dongping Lu. Transcriptional regulation of the immune receptor fls2 controls the ontogeny of plant innate immunity. *The Plant Cell*, 30:2779–2794, 2018. doi:10.1105/tpc.18.00297.